MATHEMATICS AND COMPUTATIONAL SCIENCES

Vol 2(2), 2021, pp:23-38
DOI:10.30511/mcs.2021.526850.1019
ISSN:2717-2708
http://mcs.qut.ac.ir/

QOM UNIVERSITY OF TECHNOLOGY

Numerical solution of 3-feather rose coefficient in bivariate Schrodinger Equation by rectangular FEM

M. Ghorbani[1], M. Moeini[2], M. Jamie[3]

Abstract: In this work, we approximate a typical model form of bivariate static Schrödinger Equation by an appropriate approach based on bilinear finite element method (FEM), then we obtain the results of the PDE on a new type 3 feather rose coefficient V(x, y) function in a rectangular domain i.e., eigenfunctions or solutions. In fact, we search for influence of 3-feather rose and pass by a weak singularity barrier in the origin. We also obtain approximate eigenvalues and final stiffness matrix elements. This paper is accompanied by examples of the novel Schrodinger's model.

Keywords: Rectangular and bilinear finite elements, Schrodinger equation, 3 feather rose form potential, Variable Schrodinger coefficient, Galerkin method.
2020 Mathematics Subject Classification: 35Qxx, 46F12
Received: 15 March 2021, **Accepted:** 15 April 2021

1 Introduction

Because of vast applications in basic science and technologies, during the last 50 years ago, quantum dots (QDs) have been became an encouraging field of research, and among the nanostructures, QDs have become subject of intensive experimental and theoretical studies nowadays. The improvements of the semiconductor growth techniques have offered the possibility to obtain QDs with various shapes such as spherical, cylindrical, ellipsoidal, pyramid-like, and cone-like. In recent years, a wide variety of shapes and forms, such as: quantum dots (QDs) arrays [12], conical [24], rectangular[38], cylindrical [2], disc-shaped [36], elliptical [31], lens-shaped [30], pyramidal [18], spherical [3], T-shaped [37], Y-shaped [10], etc., for the QD systems have been used. Due

[1]Corresponding author: Department of Mathematics, Qom University of Technology (QUT), Qom, Iran, ghorbani@qut.ac.ir.
[2]Department of Mathematics, Roudehen Branch, Islamic Azad University of Tehran, Roudehen, Iran, moeini@riau.ac.ir.
[3]Department of Mathematics, Qom University of Technology (QUT), Qom, Iran, mj7721004@gmail.com.

to the complicated geometric form of the shapes, the analytic solution of energy levels and wave functions are not known [20, 22].

In order to study these QDs different mathematical methods such as: variational method [11,27], 1/N expansion method [9], quantum cellular automata [15], density functional calculations [28], exact diagonalization [16], finite difference technique (FD) [8, 1], finite element method (FEM) [4,5,23,25,29,33], self-consistent Hartree method [8], k.p theory [32], Monte Carlo [35], molecular dynamics [17], Green's functions [6,14], Nikiforov–Uvarov method [26], Transfer matrix method [19] etc. have so far been used.

The finite element method (FEM) is a powerful numerical technique for solving PDEs and was originally applied to the problems in engineering, structural mechanics, applied sciences and are effective for problems with complex domain geometry. In FEM, there is a variational approach for approximating elliptic boundary value problems (BVP) such as Helmholtz and Schrodinger Equations., which try to minimize residual of the problem over a finite-dimensional subspace defined on some rectangular elements.

The basic principles underlying the FEM are relatively simple and application of this method involves some steps. One of the most important tasks in the Galerkin FEM is the division of the region into suitable non-overlapping elements. Always, the circular, semicircular and nonrectangular domain is approximated by a polygon. This generation of the mesh is particularly important for regions in 2 and 3 dimensions. First, we must partition the domain of the problem into a finite number of disjoint elements which the rectangular or triangular shapes are most common for 2D problems. For complex regions, the collection of all congruent rectangular elements should cover the original region as closely as possible. In the second step, we derive interpolation as a linear combination base functions over a typical isoperimetric or physical element by defining a complete polynomial base such as $\{1, x, y\}$ over an element. After assembling, the smooth degree of the final global polynomial, determine continuity of global approximation. In this paper, our FEM approximation belong to the space $H^1 \bigcap C^0$. In this step, we determine blocks and entries of the original stiffness matrix. In the third step, we need assemble all regular elements to obtain global matrix. In the final stage, the resulting system of equations will be solved.

In our study, we limit our discussion to a special type of the model problem [4, 5,7,21,23,25,29,33,34], and approximate a typical 2D Schrodinger Equation by means of the FEM. Finally, we evaluate the energy eigenvalues and corresponding eigenfunctions of the 3-feather rose type potential.

The structure of this paper is as follows: in Section 2, we introduce the FEM and apply it on the model problem, Section 3 we present numerical results of some examples and concluding remarks are subject of final section.

2 Application of rectangular FEM to the problem

The procedure of the FEM to solve 2D problems is as follows. We assume a 2-D linear second order Schrödinger Eq. as,

$$\begin{aligned} L\psi(x,y) &= \alpha\left(\frac{\partial^2}{\partial x^2}+\frac{\partial^2}{\partial y^2}\right)\psi(x,y)+V(x,y)\psi(x,y) \\ &= \alpha\Delta\psi(x,y)+V(x,y)\psi(x,y) \\ &= E\psi(x,y) \end{aligned} \quad (1)$$

This bivariate static Schrödinger Eq. is a linear eigenvalue problem with Dirichlet homogenous boundary conditions (BCs), the domain is rectangular $\Omega_{ph}=[a,b]\times[c,d]$ and in the normalized case, this domain can be scaled and transformed to the normalized form $\Omega_c=[0,1]\times[0,1]$. In Eq. (1), the function $V(x,y)\in H^0(\Omega_c)=L^2(\Omega_c)$ have an important role for determining geometrical confining potential and $\alpha=\frac{\hbar^2}{2m^*}$ is a given constant.

Given a general domain, we can approximate the domain by a polygon and then generate a triangulation and rectangulation over the polygon, then we can refine the mesh if necessary. We partition the domain Ω_c into some disjoint non-overlap rectangular elements and define the bilinear base functions. We assume n and m be the number of discretization points along *x* and *y* axes, so the *x* and *y* steps are $h=\frac{1}{n}$, $k=\frac{1}{m}$, and $0=x_0<x_1<\ldots<x_n=1$, $0=y_0<y_1<\ldots<y_m=1$, $x_i=a+ih$, $y_j=c+jk$. The global piecewise bilinear polynomial base functions define on the rectangular elements can be written as,

$$\varphi_{i,j}(x,y)=\begin{cases}\dfrac{x_{i+1}-x}{x_{i+1}-x_i}\dfrac{y_{j+1}-y}{y_{j+1}-y_j}, & x_i\le x\le x_{i+1}, y_j\le y\le y_{j+1}\\ \dfrac{x_{i-1}-x}{x_{i-1}-x_i}\dfrac{y_{j+1}-y}{y_{j+1}-y_j}, & x_{i-1}\le x\le x_i, y_j\le y\le y_{j+1}\\ \dfrac{x_{i-1}-x}{x_{i-1}-x_i}\dfrac{y_{j-1}-y}{y_{j-1}-y_j}, & x_{i-1}\le x\le x_i, y_{j-1}\le y\le y_j\\ \dfrac{x_{i+1}-x}{x_{i+1}-x_i}\dfrac{y_{j-1}-y}{y_{j-1}-y_j}, & x_i\le x\le x_{i+1}, y_{j-1}\le y\le y_j\\ 0, & Otherwise\end{cases} \quad (2)$$

where $i=1,2,...,n-1$, $j=1,2,...,m-1$. The node (x_i,y_j) is the vertex of 4 adjacent elements. The total number of points are equal $(1+n)(1+m)$. Since the wave functions degenerate on the boundaries, the boundary points is deleted from computing volume. Therefore, the number of unknown variables (and hence the number of algebraic equations) are equal to the number of internal discretization points $N_i=(n-1)(m-1)$.

Now, we construct the finite element approximation of the eigen wave function through piecewise linear combination of base functions by Eq. (2) on all internal nodes,

$$\tilde{\psi}(x,y)=\sum_{i=1}^{n-1}\sum_{j=1}^{m-1}u_{i,j}\varphi_{i,j}(x,y) \quad (3)$$

where $u_{i,j}$ are unknowns on (x_i,y_j) and we look for the solution in the space $C^0\bigcap H^1$. For simplicity, we use computational, normalized and isoperimetric elements by scaling and mapping $\xi=\dfrac{x-x_i}{h_x}$ and $\eta=\dfrac{y-y_j}{h_y}$. Therefore, we can rewrite the Eq. (2) as the following alternative,

$$\varphi_{i,j}(\xi,\eta)=\begin{cases}(1-\xi)(1-\eta)\ , 0\le\xi\le 1\ , 0\le\eta\le 1\\ (1+\xi)(1-\eta)\ , -1\le\xi\le 0\ , 0\le\eta\le 1\\ (1+\xi)(1+\eta)\ , -1\le\xi\le 0\ , -1\le\eta\le 0\\ (1-\xi)(1+\eta)\ , 0\le\xi\le 1\ , -1\le\eta\le 0\\ 0\qquad\qquad , \quad Otherwise\end{cases} \tag{4}$$

Since, in vicinity of each point (x_i, y_j) there are 9 points and naturally 4 proper elements, therefore in the related matrix system, there are 9 non-zero diagonal and ex-diagonal elements. So, we will have a resulting 3-diagonal block Hamiltonian matrix. Each of these blocks are 3×3 and symmetric. Now, we define residual $R(x,y)$ through substituting the linear expansion (3) into the Eq. (1),

$$R(x,y)=\alpha\Delta\tilde{\psi}(x,y)+V(x,y)\tilde{\psi}(x,y)-E\tilde{\psi}(x,y),\qquad x\in\Omega_c \tag{5}$$

The approximated wave-function $\tilde{\psi}$ is in the generalized, distributional and weak form [4,23,11], thus we can use the Galerkin weighted residual method by multiplying Eq. (5) by test functions $\varphi_{i,j}\in H^1(\Omega_c)$,

$$\int_{y_{j-1}}^{y_{j+1}}\int_{x_{i-1}}^{x_{i+1}} R(x,y)\varphi_{i,j}(x,y)dxdy=0, \tag{6-a}$$

And in the normalized space we have,

$$\int_{-1}^{1}\int_{-1}^{1} R(\xi,\eta)\varphi_{i,j}(\xi,\eta)d\xi d\eta=0, \tag{6-b}$$

In order to evaluate the equations (6), we need to use Green's theorem of second kind as [4,5,11,23], if $\Phi, U\in H^1(\Omega_c)$,

$$\iint_{\Omega}\Phi.\Delta U d\Omega+\iint_{\Omega}\nabla\Phi\bullet\nabla U d\Omega=\int_{\Gamma}\Phi.\frac{\partial U}{\partial n}d\Gamma, \tag{7}$$

Where n is the unit normal to the boundary $\Gamma=\partial\Omega$, ∇ is the gradient operator, $\Delta=\nabla.\nabla$ is the Laplacian operator and $\frac{\partial U}{\partial n}=\nabla U.n$. Due to the homogeneous boundary conditions on the entire boundary, the Eq. (7) is simplified into the form by degenerating boundary integral term,

$$\iint_{\Omega} \Phi \Delta U d\Omega = -\iint_{\Omega} \nabla \Phi \bullet \nabla U d\Omega, \tag{8}$$

Diagram (1) represents a simple description about the local nodal basis functions (2) and (4) in the vicinity of the point (x_i, y_j).

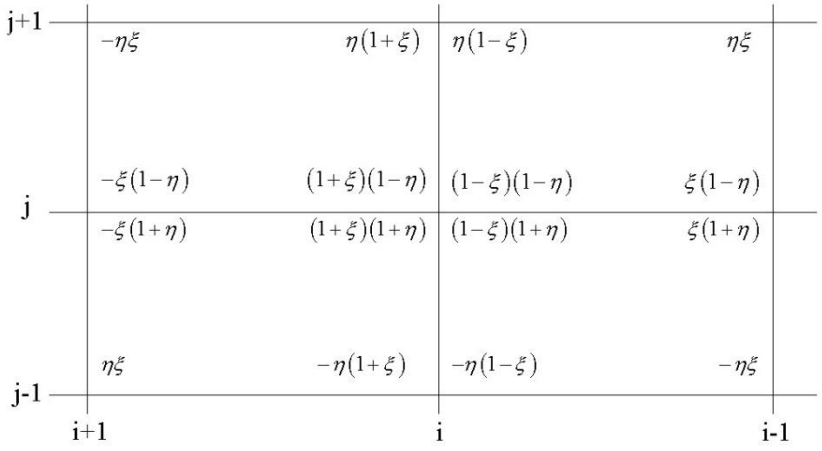

Figure 1: The 4 neighborhood elements and 9 neighborhood points of an arbitrary internal point (x_i, y_j)

Now, through integral (6), we have the following bilinear form

$$a(\tilde{\psi}, \varphi_{p,q}) = \sum_{i=1}^{n-1}\sum_{j=1}^{m-1} u_{i,j}\left(-\alpha \int_{y_{j-1}}^{y_{j+1}}\int_{x_{i-1}}^{x_{i+1}} (\nabla \varphi_{p,q} \bullet \nabla \varphi_{i,j}) dxdy + \int_{y_{j-1}}^{y_{j+1}}\int_{x_{i-1}}^{x_{i+1}} V\varphi_{i,j}\varphi_{p,q} dxdy - E\int_{y_{j-1}}^{y_{j+1}}\int_{x_{i-1}}^{x_{i+1}} \varphi_{i,j}\varphi_{p,q} dxdy\right),$$

consequently three types blocked matrices, for matrix $M_1 = \left\{ \int_{y_{j-1}}^{y_{j+1}}\int_{x_{i-1}}^{x_{i+1}} (\nabla \varphi_{p,q} \bullet \nabla \varphi_{i,j}) dxdy \right\}$, we have the entries as follows in Fig. (2).

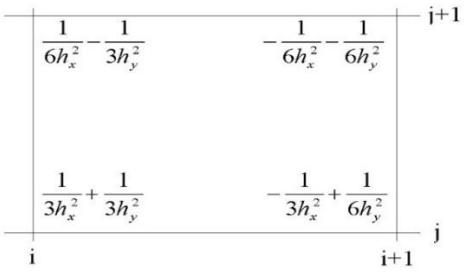

Figure 2: M_1 matrix structure and entries.

and for matrix $M_2=\left\{\int_{y_{j-1}}^{y_{j+1}}\int_{x_{i-1}}^{x_{i+1}} V\varphi_{i,j}\varphi_{p,q}dxdy\right\}$, the entries are as follows in Fig. (3).

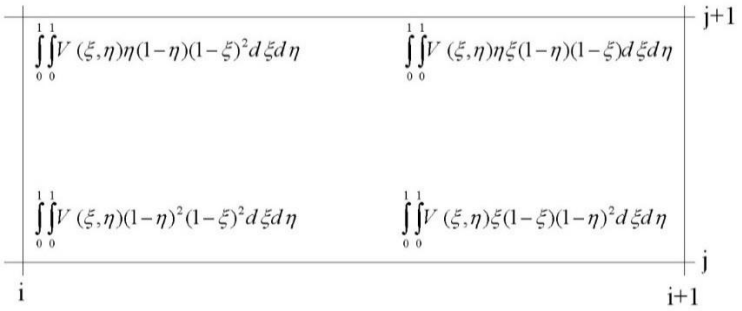

Figure 3: M_2 matrix entries.

and for the third matrix $M_3=\left\{\int_{y_{j-1}}^{y_{j+1}}\int_{x_{i-1}}^{x_{i+1}} \varphi_{i,j}\varphi_{p,q}dxdy\right\}$ the entries are as Fig. (4).

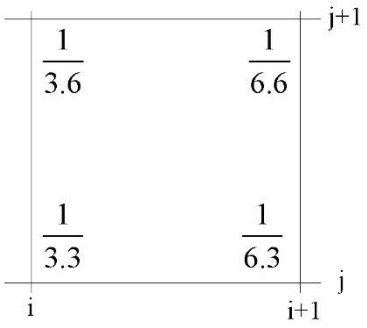

Figure 4: M_3 matrix elements.

After evaluating above mentioned sub-matrices by assembling uniform elements and use row-wise ordering for the nodal points , we get the following eigenvalue system,

$$-\alpha M_1\psi + M_2\psi = EM_3\psi, \qquad \text{(9-a)}$$

$$M_3^{-1}(-\alpha M_1\psi + M_2\psi) = E\psi, \qquad \text{(9-b)}$$

Where, E s are energy eigenvalues. There are many direct or indirect methods such as SOR, to solve above stiff system (9).

3 Numerical results and discussions

By using the FEM and a compact density matrix formalism, we investigate properties of 3-rose flower discontinuous type V . Figure (5) shows the mentioned 3 feather abloom potential V ,

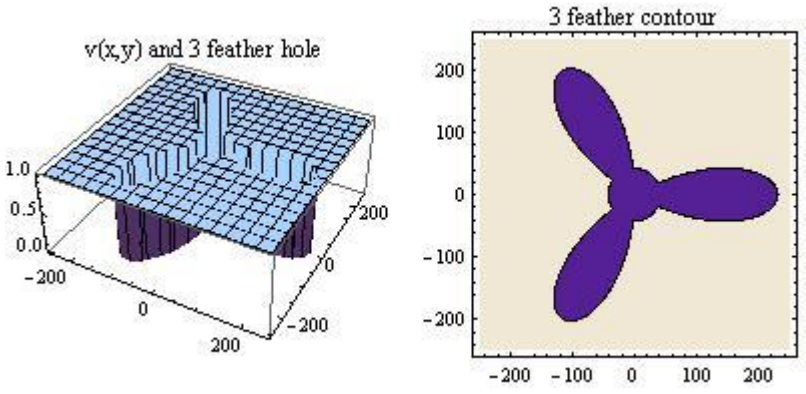

Figure 5: The diagram of the confining 3 feathers rose potential $V=0$ in the rose and $\gamma(=1)$ otherwise, 3D perspective and contour plot of the potential, the domain $\Omega_{ph}=[250,250]\times[250,250]$, the potential can be gotten by the equations: $r=Cos(3\theta)$ or $r=Sin(3\theta)$, and the potential is zero in the 3-rose area loop and is 0 otherwise, the radius of the small interior circle is $\frac{1}{\sqrt{30}}$.

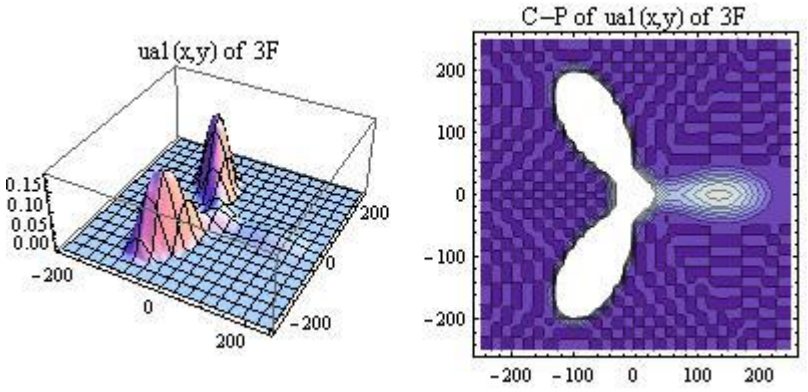

Figure 6: The 3D and contour plot of the eigen-function approximation $\tilde{\psi}$, correspond to the minimum eigenvalue $\lambda_{\min}=0.0408444$, under conditions $n=m=30$, $\alpha=25.0$, $\gamma=1$, 30^2 uniform elements, the radius of the small interior circle that is $\frac{1}{\sqrt{30}}$ for prevention of singularity.

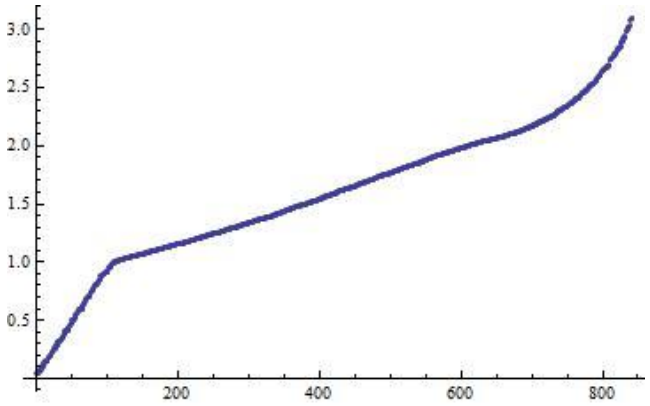

Figure 7: The data plot of the eigenvalues λ_i, $n=m=30$, $\alpha=25$, 30^2 elements, $\lambda_{\min}=0.040844$ and $\lambda_{\max}=3.0928$, the square domain size is fix, the pointwise data graph is increasing, the condition number of the stiffness matrix can be computed by $\left|\frac{\lambda_{\min}}{\lambda_{\max}}\right|$ which shows a measure of ill conditioning.

In physical interpretation, the 3D figure of 3-feather rose hole in the rectangular domain, indicate the distribution of the probability densities inside the quantum structure. This probabilities show the probability of finding an electron in an assumed structures and therefore can provide us information about the free careers distribution. We also find that the energy decreases by increasing domain size.

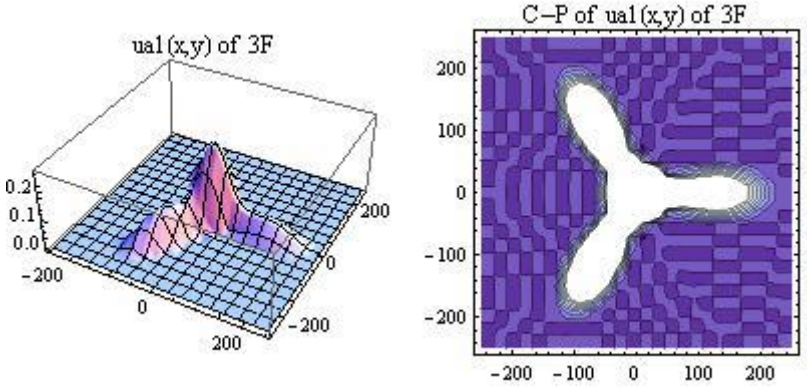

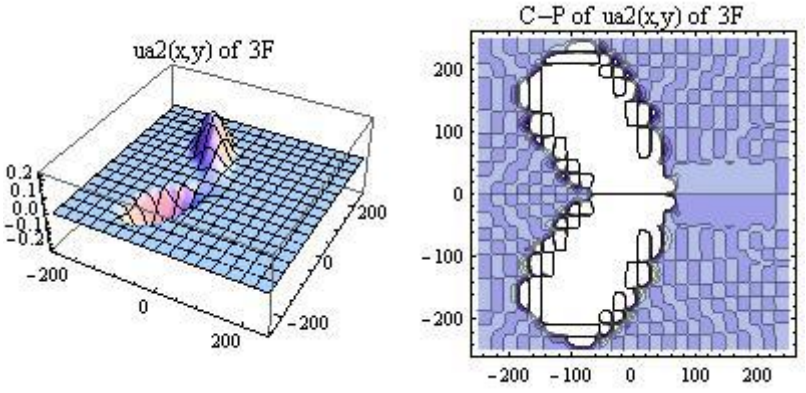

Figure 8: The first two approximate eigenfunctions ψ, 3-feather rose V, $n=m=25$, $\alpha=25$, $\gamma=1$, $\lambda_{\min}=0.038936$ and $\lambda_1=0.042003$, $N_i=24^2$, the radius of the small interior circle is equal to $\frac{1}{\sqrt{20}}$.

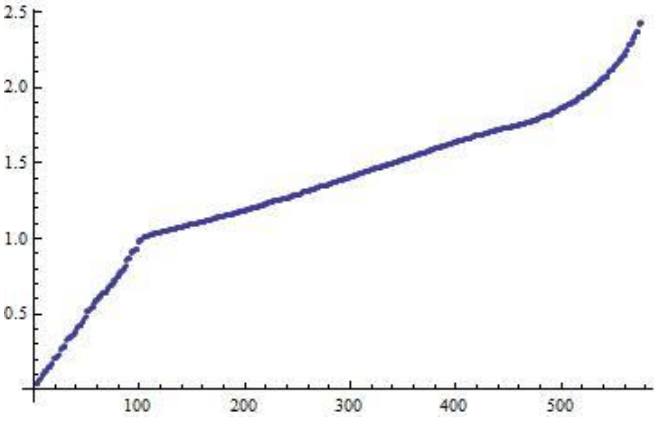

Figure 9: The data graph of the eigenvalues λ_i, $n=m=25$, $\alpha=25$, 25^2 elements, $\lambda_{\min}=0.038936$ and $\lambda_{\max}=2.432915$, the domain size is fix, the radius of the small interior circle is equal $\frac{1}{\sqrt{20}}$.

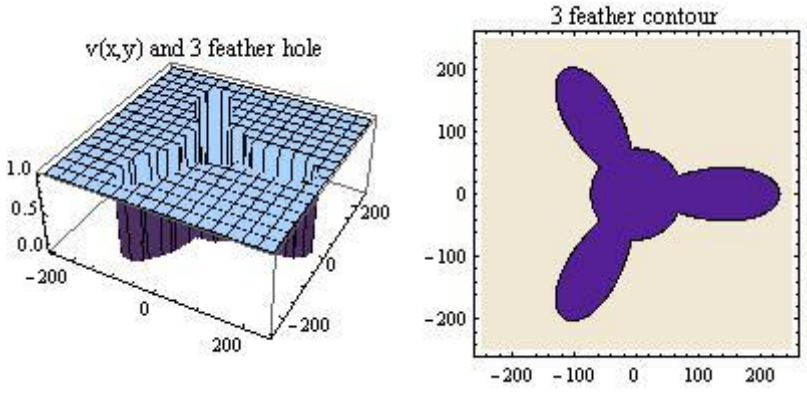

Figure 10: The graph of the confined potential V , 0 in the 3 feathers rose and inner circle, and unity otherwise, the 3D perspective and the contour plot, the domain size is $\Omega = [250, 250] \times [250, 250]$, this rose can be gotten by changing $r = Cos(3\theta)$ or $r = Sin(3\theta)$ from polar to rectangular coordinate, the radius of the small interior circle is equal $\frac{1}{\sqrt{10}}$.

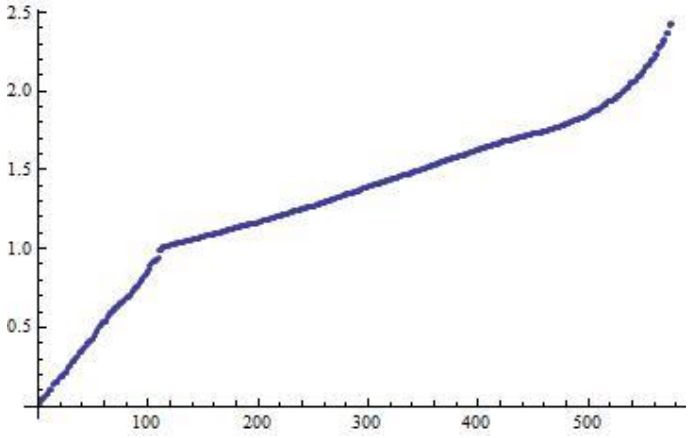

Figure 11: The pointwise graph of the eigenvalues λ_i , $n = m = 25$, $\alpha = 25.0$, 25^2 elements, $\lambda_{\min} = 0.021899$ and $\lambda_{\max} = 2.430496$, the domain size is fix, the radius of the small interior circle is equal $\frac{1}{\sqrt{10}}$.

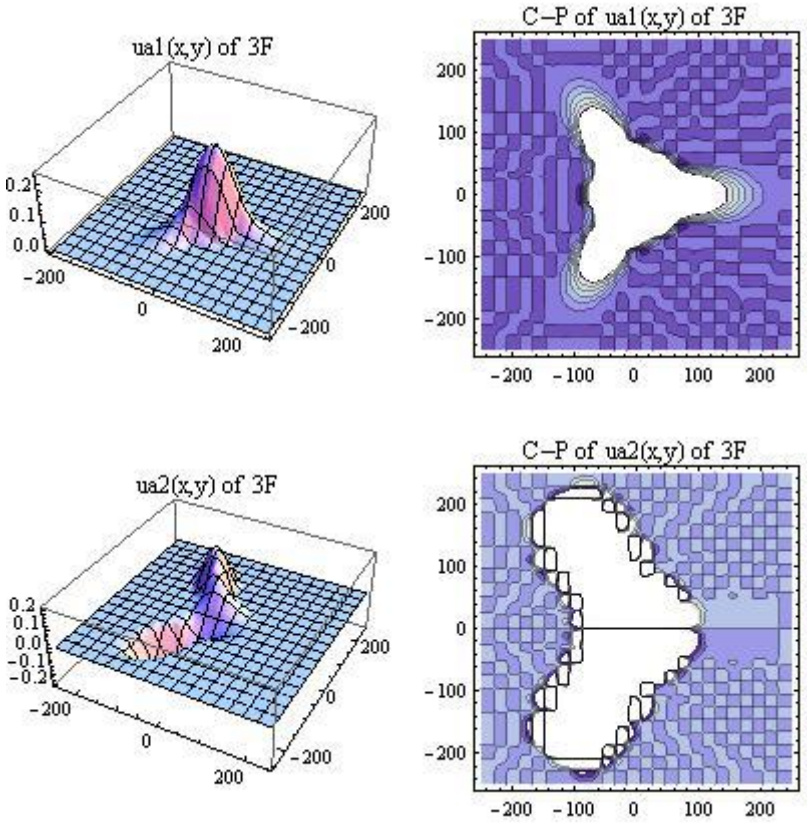

Figure 12: The graph of the first 2 eigenfunctions ψ, 3 feather hole potential V, $n=m=25$, $\alpha=25$, these graphs correspond to the eigenvalues $\lambda_{\min}=0.021899$ and $\lambda_{\max}=2.430496$, and $N_i=24^2$, the radius of the small interior circle is equal to $\frac{1}{\sqrt{10}}$

4 Concluding remarks

In this work, we get some approximate eigenvalues of the model problem, and the last two approximate value of the Schrodinger PDE correspond to the last two minimum eigenvalues. We can investigate the electronic properties of multi-feather nanoflower, by using the FEM, finite difference method (FDM)[1], meshless methods[13] etc, we can get effect of any change in the domain size, in the radius of small interior circle and any

change on the parameters. We can also show that a nonlinear behavior in the energy value is observed when the number of feathers increased ($r = Cos(n\theta)$). In most of complex models, analytic solution do not exist, therefore to analyze the error, have complexity and so error analysis of this work is subject of another paper. The application of the radial base functions (RBFs) and meshless methods, is another future struggle of us. In present work, instead of Galerkin method, we can use of another weighted residual such as Petrov Galerkin with different and smooth test functions such as Hermite type. In our numerical experience, triangular elements, will give better approximation than rectangular elements.

References

[1] W.F. Ames, Numerical Methods for Partial Differential Equations, 3Ed, Academic Press, 1992.

[2] G. Bester, A. Zunger, Cylindrically shaped zinc-blende semiconductor quantum dots do not have cylindrical symmetry: Atomistic symmetry, atomic relaxation, and piezoelectric effects, Physical Review B, 71(4) 2005, 045318.

[3] C. Bose, Binding energy of impurity states in spherical quantum dots with parabolic confinement, Journal of Applied Physics, 83(6) 1998, 3089-3091.

[4] D. Braess, Finite Elements, Theory, Fast Solvers, and Applications in Elasticity Theory, Cambridge Univ. Press, 2007.

[5] S. Brenner, R. Scott, The Mathematical Theory of Finite Element Methods, Springer, 2007.

[6] P.K. Chattopadhyay, Mathematical Physics, New Age Int. (P) Ltd., 1990.

[7] D.M. Cunha, F.L. Souza, Facile synthetic route for producing one-dimensional zinc oxide nanoflowers and characterization of their optical properties, Journal of Alloys and Compounds, 577 2013, 158-164.

[8] A. Deyasi, S. Bhattacharyya, N.R. Das, Computation of intersubband transition energy in normal and inverted core–shell quantum dots using finite difference technique, Superlattices and Microstructures, 60 2013, 414-425.

[9] M. El-Said, Spectroscopic structure of two interacting electrons in a quantum dot by the shifted 1/N expansion method, Physical Review B, 61(19) 2000, 13026.

[10] T.F. Fang, S.J. Wang, Cross correlations and shot noise in a Y-shaped quantum dot, Journal of Physics: Condensed Matter, 19(2) 2006, 026204.

[11] B.A. Finlayson, The Method of Weighted Residuals and Variational Principles, with application in fluid mechanics, heat and mass transfer, Academic Press, 1972.

[12] T. García, Francisco Manuel Gómez-Campos, and Salvador Rodríguez-Bolívar, Influence on miniband structure of size variations in regimented InAs/GaAs quantum dots arrays, Journal of Applied Physics, 114 2013, 064311.

[13] M. Ghorbani, Diffuse Element Kansa Method, Applied Mathematical Sciences, 4(12) 2010, 583-594.

[14] V. Golubnychiy, H. Baumgartner, M. Bonitz, A. Filinov and H. Fehske, Screened Coulomb balls-structural properties and melting behavior, Journal of Physics A: Mathematical and General, 39(17) 2006, 4527.

[15] M. Governale, M. Macucci, G. Iannaccone, C. Ungarelli, and J. Martorell, Modeling and manufacturability assessment of bistable quantum-dot cells Journal of applied physics, 85(5) 1999, 2962-2971.

[16] A.D. Gu¨c¸lu¨, Q.F. Sun, H. Guo, R. Harris, Geometric blockade in a quantum dot: Transport properties by exact diagonalization, Physical Review B, 66(19) 2002, 195327.

[17] A.D. Güçlü, C.J. Umrigar, Maximum-density droplet to lower-density droplet transition in quantum dots, Physical Review B 72(4) 2005, 045309.

[18] T.M. Hwang, W. Wei Lin, W.C. Wang, Weichung Wang, Numerical simulation of three dimensional pyramid quantum dot, Journal of Computational Physics, 196(1) 2004, 208.

[19] S.M. Ikhdair, M. Hamzavi, A quantum pseudodot system with two-dimensional pseudoharmonic oscillator in external magnetic and Aharonov-Bohm fields, Physica B: Condensed Matter, 407(21) 2012, 4198-4207.

[20] R. Khordad, H. Bahramiyan, Impurity position effect on optical properties of various quantum dots, Physica E: Low-dimensional Systems and Nanostructures, 66 2015, 107-115.

[21] Y.J. Kim, J. Yoo, B.H. Kwon, Y.J. Hong, C.H. Lee and G.C. Yi, Position-controlled ZnO nanoflower arrays grown on glass substrates for electron emitter application, Nanotechnology 19(31) 2008, 315202.

[22] M. Mardaania, A. Shokri, K. Esfarjani, Analytical results on coherent conductance in a general periodic quantum dot: Transfer matrix method, Physica E: Low-dimensional Systems and Nanostructures, 28(2) 2005, 150-161.

[23] J.T. Marti, Introduction to Sobolev spaces and finite element solution of elliptic boundary value problems, Academic Press, 1986.

[24] R.V.N. Melnik, M. Willatzen, Bandstructures of conical quantum dots with wetting layers, Nanotechnology, 15(1) 2004.

[25] A.R. Mitchell, R. Wait, Finite Element Analysis and Applications, John Wiley, 1985.

[26] M.A. Naser, M.J. Deen, D.A. Thompson, Spectral function and responsivity of resonant tunneling and superlattice quantum dot infrared photodetectors using Green's function, Journal of Applied Physics, 102(8) 2007, 083108.

[27] A.V. Nenashev, and A. V. Dvurechenskii, Variational method of energy level calculation in pyramidal quantum dots, Journal of Applied Physics, 127(15) 2020, 154301.

[28] S. Nomura, Y. Aoyagi, Density of states of a quantum dot array probed by photoluminescence spectra, Surface science, 529(1-2) 2003, 171-179.

[29] J.N. Reddy, An Introduction to the Finite Element Method, Mc Graw-Hill, 2005.

[30] A.H. Rodrıguez, H.Y. Ramırez, Analytical calculation of eigen-energies for lens-shaped quantum dot with finite barriers, The European Physical Journal B, 66(2) 2008, 235-238.

[31] E. Sadeghi, F. Vahdatnejad, M. Moradi LM, Effect of polarization charges on impurity binding energy in elliptical quantum wire, Superlattices and Microstructures, 58 2013, 165-170.

[32] V.A. Shuvayev, L.I. Deych, I.V. Ponomarev, A.A. Lisyansky, Self-consistent Hartree method for calculations of exciton binding energy in quantum wells, Superlattices and Microstructures, 40(2) 2006, 77-92.

[33] P. Solín, Partial Differential Equations and the Finite Element Method, 2005, John Wiley & Sons.

[34] L. Song, A. Lukianov, D. Butenko, H. Li, J. Zhang, M. Feng, L. Liu, D. Chen and N.I. Klyui, Facile Synthesis of Hierarchical Tin Oxide Nanoflowers with Ultra-High Methanol Gas Sensing at Low Working Temperature, Nanoscale Research Letters, 14(1) 2019, 1-11.

[35] O. Stier, M. Grundmann, D. Bimberg, Electronic and optical properties of strained quantum dots modeled by 8-band k.p theory, Physical Review B, 59(8) 1999, 5688.

[36] R. Wei, W. Xie, Optical absorption of a hydrogenic impurity in a disc-shaped quantum dot, Current Applied Physics, 10(3) 2010, 757-760.

[37] B.H. Wu, J.C. Cao, Interference of conductance and shot noise properties of photon-assisted transport through a T-shaped double quantum dot, Physical Review B, 73(20) 2006, 205318.

[38] G. Zhou and Y. Li, Electromagnetic-field-induced resonant structures for an open rectangular quantum dot, The European Physical Journal B-Condensed Matter and Complex Systems, 46(1) 2005, 127-132.